

Provided for non-commercial research and education use.
Not for reproduction, distribution or commercial use.



This article appeared in a journal published by Elsevier. The attached copy is furnished to the author for internal non-commercial research and education use, including for instruction at the authors institution and sharing with colleagues.

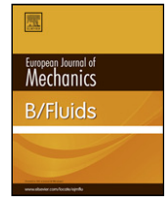
Other uses, including reproduction and distribution, or selling or licensing copies, or posting to personal, institutional or third party websites are prohibited.

In most cases authors are permitted to post their version of the article (e.g. in Word or Tex form) to their personal website or institutional repository. Authors requiring further information regarding Elsevier's archiving and manuscript policies are encouraged to visit:

<http://www.elsevier.com/copyright>

Contents lists available at [SciVerse ScienceDirect](http://SciVerse.ScienceDirect.com)

European Journal of Mechanics B/Fluids

journal homepage: www.elsevier.com/locate/ejmflu

The fluid dynamics of the rotating flow in a Tesla disc turbine

Abhijit Guha^{*}, Sayantan Sengupta

Mechanical Engineering Department, Indian Institute of Technology Kharagpur, Kharagpur 721302, India

ARTICLE INFO

Article history:

Received 11 October 2011

Received in revised form

19 June 2012

Accepted 23 August 2012

Available online 14 September 2012

Keywords:

Tesla turbine

Coriolis

Centrifugal

Viscous

Pathline

Flow reversal

ABSTRACT

The flow induced by rotating discs has attracted some of the greatest minds in fluid dynamics like von Kármán and Batchelor, and still is a vigorously active research area. In comparison, the available analysis of the rotating flow in the narrow gaps among closely-spaced co-axial multiple discs of a Tesla turbine, which produces power, is limited. In this paper a simple theory has been presented that describes the three-dimensional fields of velocity and pressure in the Tesla disc turbine. The theory gives the torque and power output which have been verified by comparing the theoretical predictions with recently published experimental results. The governing conservation equations have been cast in a form that makes it possible to formulate analytical solutions and to develop clear physical interpretation for each term in the equations. Thus the roles of each of the centrifugal, Coriolis, inertial and viscous forces in generating torque and power, and in establishing the pressure field have been comprehensively investigated and explained here. This physical exposition of the rotating flow in a Tesla disc turbine has been achieved for the first time in the present paper. Several subtle flow physics and fluid dynamic behaviors have been elucidated. As an example, it is shown here that a Tesla disc turbine may generate net torque and power even when the tangential fluid speed at the disc periphery is less than the local tangential speed of the disc. The subtle role of the Coriolis acceleration in establishing such flow conditions, which involve flow reversal and complex pathlines, has been explained.

© 2012 Elsevier Masson SAS. All rights reserved.

1. Introduction

The Tesla disc turbine is a kind of turbo-machinery in which the rotor is constructed by a series of co-axial, parallel flat discs rather than blades. This bladeless turbine was invented by the famous scientist Nikola Tesla [1]. The discs are arranged such that a small gap is maintained between any two successive discs, and they are attached to a central shaft. The combination of discs and shaft is placed inside a cylindrical casing with a small radial and axial clearance. One or more nozzles are used to guide the working fluid to enter nearly tangentially from the periphery of the discs. There are exit ports near the shaft at the center of each disc. As the fluid passes through the narrow gaps between the discs it approaches in a spiral path (usually, but see the new findings regarding complex non-spiral relative pathlines in Section 4). The working fluid travels from the inlet up to the central exit due the difference of pressure between the periphery and the central exit, and the component of inward radial velocity. The radial velocity gradually increases towards the central exit due to the gradual decrease of flow area. On the other hand, from inlet to exit, the tangential velocity may

increase or decrease, depending on the local balance of various components of forces (see Section 3).

Initially the Tesla turbine did not have much commercial success and eventually succumbed to other emerging types of turbines. Research into Tesla turbines has however been conducted since the 1950s [2,3] and recently there has been a resurgence of interest [4]. The main disadvantage of the Tesla disc turbines is that the present values of their efficiency are lower than that of conventional turbines. Tesla turbines, however, have several advantages (mentioned below) and may find niche applications in the future. Moreover, it is hoped that the current surge of research would improve the efficiency of the disc turbines – reference [5], for example, has developed an improved design of the nozzle, greatly improving the efficiency and achieving uniformity in the velocity profile of the jet. (The loss in the nozzle is generally recognized [3,6] as a major source of loss in a conventional Tesla turbine.)

The Tesla disc turbine is simple to manufacture and is less expensive. It is capable of generating power for a variety of working media like Newtonian fluids, non-Newtonian fluids, mixed fluids and particle-laden two-phase flows (many aspects of two-phase flow may be found in Refs. [7–11]). The turbine has a self-cleaning nature due the centrifugal force field. This makes it possible to operate the turbine in case of non-conventional fuels like biomass which produce solid particles. It also suggests that this bladeless turbine may be well suited to generate power in geothermal power stations [12].

^{*} Corresponding author. Tel.: +91 3222281768; fax: +91 3222282278.

E-mail addresses: a.guha@mech.iitkgp.ernet.in, guha.a@rediffmail.com (A. Guha).

Nomenclature

$a_{C,\theta}$	θ -component of Coriolis acceleration
$a_{C,r}$	r -component of Coriolis acceleration
$a_{CF,r}$	r -component of centrifugal acceleration
$a_{F,\theta}$	θ -component of viscous acceleration
$a_{F,r}$	r -component of viscous acceleration
a_H	$\equiv \frac{V_r V_\theta}{r}$
$a_{I,r}$	r -component of inertial acceleration
b	Gap between the two discs
k	Isentropic coefficient of fluid
p	Pressure
P	Modified pressure = $p - \rho g_z z$
p'	Non dimensional pressure = $\frac{p-p_2}{\rho \Omega^2 r_2^2}$
r	Radial coordinate
R	Radius ratio = $\frac{r}{r_2}$
U	Absolute velocity of fluid
V	Relative velocity of fluid
\dot{W}_{th}	Theoretical ideal power output
\dot{W}_{loss}	Overall loss in Tesla turbine
\dot{W}_{act}	Theoretical power output with loss
z	Axial coordinate
γ	Tangential speed ratio = $\frac{\bar{U}_{\theta 2}}{\Omega r_2}$
$\Delta \bar{V}_\theta$	$\equiv \frac{(\bar{V}_\theta - \bar{V}_{\theta 2})}{\Omega r_2}$
Δp_{ic}	Pressure drop between inlet and central exit of the rotor
ζ	Non dimensional average relative tangential velocity = $\frac{\bar{V}_\theta(r)}{\bar{V}_{\theta 2}}$
ζ_m	Modified ζ
θ	Azimuthal direction in cylindrical coordinate system
μ	Viscosity of the working fluid
ν	Kinematic viscosity of working fluid (here the fluid is air)
ξ	Non dimensional average relative radial velocity = $\frac{\bar{V}_r(r)}{\bar{V}_{r 2}}$
ρ	Density of the working fluid
τ_w	Wall shear stress on one side of a single disc
ϕ_2	$\equiv \frac{\bar{V}_{r 2}}{\Omega r_2}$
Ω	Rotational speed of the disc
Ω_{steady}	Steady state rotational speed of the disc
\mathfrak{S}	Torque on one side of a single disc
\mathfrak{S}_{tot}	Total torque
Subscripts	
r	Component along the r direction
z	Component along the z direction
θ	Component along the θ direction
1	Central exit of the rotor
2	At rotor inlet
Overbar	
$(\bar{\quad})$	z -averaged (z varies from 0 to b) flow variables

In this paper a theory is described that gives the three-dimensional fields of velocity and pressure in the Tesla disc turbine. The presented theory also gives the torque and power output which have been verified by comparing the theoretical predictions with recent experimental measurements [13]. (All experimental

results and numerical illustrations of the theory given in this paper are for air as the working fluid.) By a systematic order of magnitude analysis, the dominant terms have been retained in the governing conservation equations. This has made it possible to formulate analytical solutions and to develop clear physical interpretation for each term in the equations. Thus the roles of each of the centrifugal, Coriolis, inertial and viscous forces in generating torque and power and in establishing the pressure field have been comprehensively investigated and explained here. This physical exposition of the rotating flow in a Tesla disc turbine has been achieved for the first time in the present paper.

1.1. Previous work on Tesla disc turbines and related issues

Rice [6] in his article “Tesla turbomachinery” had described the advances of research (up to 1991) in the field of the Tesla turbine. There are two old approaches which are worth mentioning: the truncated series substitution methodology [14] and the bulk parameter analysis [15,16,3]. The problem of using truncated series substitution methodology is its lower accuracy; the bulk parameter approach is not useful because of the inadequacy of the friction factor concept [6]. A simple but very effective method for measuring the net power output and overall loss (the bearing and other losses), called the “angular acceleration method”, has been developed and fully described by Hoya and Guha [4]. This proved to be a successful method for overcoming many difficulties associated with the determination of very low torque at very high angular speed. The reference gives detailed measurements and operational experience for Tesla disc turbines. It has previously been recognized that the performance of the nozzle and the inlet is a limiting factor for the overall efficiency of such turbines. Rice [6] wrote: “In general, it has been found that the efficiency of the rotor can be very high, at least equal to that achieved by conventional rotors. But it has proved very difficult to achieve efficient nozzles in the case of turbines. [...] As a result, only modest machine efficiencies have been demonstrated”. Through a systematic study of the major sources of loss, Guha and Smiley [5] developed a new design of nozzle-inlet assembly that reduces the loss tremendously and substantially improves the uniformity of the velocity profile in the jet. The analysis and design [5] therefore addresses and solves a major issue in the design of Tesla disc turbines that seems to have seriously affected their development for over 50 years.

Several studies have been conducted in the past two decades on various aspects of Tesla disc turbines.¹ Couto et al. [17] presented a simple calculation procedure for estimating the number of discs required inside the Tesla turbine to accomplish a prescribed job. Their calculation is based on the estimation of boundary layer thickness of the rotating fluid on the rotating disc. They assumed that for laminar flow $\delta \approx 5\sqrt{\nu(r_2 - r_1)/U_\theta}$ (δ is the boundary layer thickness) though using the absolute tangential velocity for calculation of the boundary layer thickness for a relative rotational reference frame may not be appropriate. Furthermore their calculation had no experimental or numerical verification. Valente [18] claimed that a Tesla turbine can be used successfully in gas liquefaction plants for pressure reduction of hydrocarbon gases. According to them gas liquefaction can be done nearly isothermally by the use of a Tesla turbine. Deam et al. [19]

¹ One of the reviewers has drawn our attention to some performance curves of Tesla disc turbines that are available on the Web: numerical results of Tahil are available at <http://www.stanford.edu/~hydrobay/lookat/tt.html#ref1b>, and experimental results of Lezsovits on a Tesla turbine working on biomass fuel are available at <http://mycite.omikk.bme.hu/doc/40405.pdf>. Details of the numerical or experimental procedure are however not given and these results have not been formally published.

attempted to develop a simple analytical model of a Tesla turbine considering incompressible and one dimensional flow. A limitation of their theory is the absence of the radial flow feature. Moreover their theory aims to predict only the no-loss maximum efficiency of the turbine which is attainable when the rotor velocity is equal to the velocity of the working fluid. This, however, does not happen in reality because, if there is no relative velocity between the disc-rotor and the working fluid, the viscous drag force will be zero and in consequence, there will be no power output. Carey [20] explored the fact that a Tesla turbine can be used as an expander (cheap, durable and robust) for solar Rankine cycle combined heat and power systems. He found the efficiency of the turbine by a one-dimensional idealized momentum transfer model. According to him, under optimal design conditions, 75% isentropic efficiency of this turbine can be achieved. Lampart et al. [21] discussed the use of a Tesla turbine in a co-generating micro-powerplant. Choon et al. [22] developed a Tesla turbine for generation of power utilizing the potential energy from the household water supply. Moreover, they have conducted an optimization study by using the CFD software package and observed that their design yields a torque of .033 N m with an overall efficiency of 10.7%.

The theoretical treatments for the flow between the discs of a Tesla turbine usually assume that the flow is laminar. However, this assumption is doubtful when the pressure drop across the rotor is high. A detailed stability study is necessary to find out the applicability of a laminar theory. A number of situations for the transition of rotating flow between two discs are described in the literature. Gregory et al. [23] and Faller and Kaylor [24] described two types of instabilities of the boundary layer over an infinite rotating disc. The first type, denoted as class A (or type II) is because of viscous instability and the second type denoted as class B (or type I) is because of inflectional instability. Both of the instabilities appear inside the boundary layer in the form of regular systems of spiral rolls although they are different in orientation, phase velocity and wavelength. Savas [25,26] had observed two types of instabilities in the form of circular and spiral rolls (which correspond to type 2 and type 1 instabilities [27]) in the Bödewadt layer. Instability of flow between a rotating disc and a stationary disc with separated boundary layers appears in the form of inward propagating circular waves [28]. With the increase of Reynolds number instability of spiral pattern coexists with circular waves [28,29]. Instability of flow between a rotating disc and a stationary disc with merged boundary layer appears in the form of localized spots or of solitary waves [30]. With the increase of Reynolds number a number of these turbulent structures are superimposed on a short-wavelength spiral pattern. Gauthier et al. [31] observed two types of instability patterns (axisymmetric propagating vortices, positive spirals) in co and weak counter-rotating flows, while for the case of highly counter-rotating flows they found a third type (which appears as negative spirals). According to them, the instability patterns for the case of co and weak counter-rotating flows are qualitatively the same as compared to the rotor-stator systems, but negative spirals are specific to highly counter-rotating flows.

The above stability studies may not be directly applicable to Tesla turbines because the basic flow is different. Murata et al. [32] observed in their experiment that the flow inside the disc gap of a Tesla disc pump is always laminar except for a small region near the inner and outer periphery. According to Rice [6], laminar flow, laminar flow with regions of recirculation, fully turbulent flow, transition flow, and reverse transition flow can be observed for flow between the discs of a Tesla turbine. Rice [6] cited the conclusion of Wu [33] that viscoelastic number (proposed by Nendl) most adequately characterizes the flow regimes; Wu had concluded this by considering all available experimental and analytical evidences. According to Nendl [34,35], the flow remains

laminar if the viscoelastic number is less than 10, where viscoelastic number = $[(V_r b^2)/(vr)]$. The stability analysis for flow between the discs of a Tesla turbine has not been performed thoroughly yet. A quantitative analysis however is required for establishing the regime where the flow between the narrow disc-space of the Tesla turbine remains laminar.

1.2. Previous work on rotating fluid flow in contact with discs

The fluid flow in contact with a rotating disc has been the subject-matter of many previous studies, both theoretical and experimental. The problem has attracted some of the greatest minds in fluid dynamics such as von Kármán and Batchelor, new investigations are still being reported (see below). Several of these contributions have been described below for their relatedness, but the flow within the small gap between two co-rotating discs is quite different from the flow in an infinite or large expanse of fluid. Additionally, the much explored subject usually concerns the development of fluid flow as a result of externally-driven disc rotation, whereas in a Tesla turbine the disc rotates (and delivers shaft power output) as a result of the action of fluid flow (usually in the form of a nearly-tangential jet at the periphery).

The study of rotating flow is important in order to understand scientific fields like oceanography, geophysics, astrophysics, fluid machinery etc. The pioneer in this field was Ekman [36] who had studied the influence of the earth rotation on ocean currents. Using similarity analysis, von Kármán [37] deduced the steady-state solution for the effect of rotation of a single disc of infinite radius in a quiescent fluid. The effect of rotation of the disc on the fluid is that the fluid just next to the disc moves radially outward due to the centrifugal force, and to fill the gap the fluid from above moves axially towards the disc. Bödewadt [38] had studied a case which was just opposite to that of von Kármán [37]. The aim of his analysis was to find the effect of the presence of a static disc (which will not rotate) in a fluid which is rotating initially like a rigid body. In this case, the rotating flow just next to the static disc encounters the effect of friction of the disc and therefore this region turns into a slow velocity zone, because of the centripetal force an inward fluid flow sets up, which ultimately has to move axially upwards (opposite to the direction of the disc).

Batchelor [39] had studied a case where instead of one disc, there were two discs (with infinite radius) separated by a distance. One of the discs rotated at a constant angular speed while the other disc was static. The motion to the initially static fluid is imparted by the rotating disc. The solutions given by Batchelor [39] show the existence of boundary layers on both the rotor and the stator, and between these two layers there is a core of fluid which rotates at an angular velocity less than that of the rotating disc. Furthermore, Batchelor's solution shows that a radial inflow near the stator surface supplies fluid to the core while the core has to supply fluid axially towards the rotating disc which continuously pumps the fluid radially outward. Investigating the same problem by series expansion for flow with small Reynolds number, Stewartson [40] arrived at a different solution and conclusion as compared to those of Batchelor [39]. According to Stewartson [40], the flow structure in between the two discs does not contain a Batchelor-type core region at all, the flow rather resembles more the von Kármán-type solution of a rotating disc in an infinite expanse of fluid, and the Stewartson solution gives a continuous reduction of the angular speed of the fluid from the rotating to the static disc.

Picha and Eckert [41] sought to resolve the dichotomy of the Batchelor–Stewartson theoretical solutions through conducting experiments. The discs used in the experiment were necessarily of a finite size and two configurations were used – in one of them the spacing between the two discs at the outer radius was kept open to the atmosphere, in the other the aforementioned space was sealed

from the atmosphere with the help of a shroud. Most interestingly, they found in their experiment that the solution of Stewartson [40] is valid when the wheel space is open to the atmosphere and the solution of Batchelor [39] is valid when there is a stationary shroud at the outer radius.

However, the experiment by Picha and Eckert [41] did not settle the Batchelor–Stewartson controversy conclusively and a very large number of investigators have examined the problem from various angles and by several means - experimental, theoretical and computational. A summary of this evolution in the thought process is presented in the next two paragraphs before explaining the current knowledge about the multiplicity of the solutions (of which the Batchelor and the Stewartson solutions are just two particular cases).

Numerical solutions given by Lance and Rogers [42] indicate that the Batchelor [39] flow with separated boundary layers evolves towards a purely viscous flow with merged boundary layers, when the Reynolds number (i.e. $\Omega h^2/\nu$) is decreased (h is the gap between the two discs) - this would suggest a transition towards the Stewartson-type flow when the Reynolds number is low. Pearson [43], on the other hand, also on the basis of numerical solutions, pointed out that the small Reynolds number trend proposed by Stewartson [40] is misleading and the Batchelor [39] solution is qualitatively correct. Sirivat [44] showed that as the Reynolds number decreases and the disc radius becomes infinite, the flow becomes a viscous torsional Couette flow.

The experimental studies of Gauthier et al. [45] and the numerical studies of Dijkstra and van Heijst [46] add another level of complexity in that their results show that for large values of Reynolds number and finite geometry of the discs (enclosed by a side wall) the angular velocity of the core is a function of the radial coordinate and hence, it deviates from the self-similar solution given by Batchelor [39]. Zandbergen and Dijkstra [47], Poncet et al. [48,49] pointed out that the flow structure in a rotor–stator system is also dependent on the superposed flow into the cavity. According to Poncet et al. [49], with an increase of superposed outflow the Batchelor [39] model with a rotating core turns into the Stewartson [40] model with no or very little core rotations.

This brings one to the existence of multiple solutions. Dijkstra and van Heijst [46] showed numerically and experimentally the coexistence of a Stewartson type flow and a Batchelor type flow for counter-rotating discs. They observed the Stewartson type flow near the center and the Batchelor type flow near the periphery of the discs. Mellor et al. [50] had shown that at a fixed Reynolds number many solutions are possible for the flow between two discs, and that when the Reynolds number becomes very large the von Kármán solution (obtained originally for a single disc in an infinite expanse of fluid) is obtained as the limiting case of a certain branch of two disc solutions. Rogers and Lance [51] and many others later (e.g. Zandbergen and Dijkstra [47]) have shown that the Batchelor and the Stewartson flows are the two of many solutions that progressively appear as the Reynolds number is increased. The multiplicity of steady state solutions for the flow between two rotating discs has been extensively studied by Holodniok et al. [52,53]. They had considered three distinct cases: two discs rotating in the same direction, two discs rotating in the opposite direction, and, one disc rotating while the other one is kept stationary.

It is thus clear from the above discussion that the various flow structures resulting from the interaction of a fluid and solid discs have been studied extensively. We therefore now explain why the rotating flow within the Tesla disc turbines is novel and not covered by the previously discussed studies of solid–fluid interaction. Like the Batchelor [39] or the Stewartson [40] flows, the flow in the Tesla disc turbine also takes place within the gap between two discs. However, unlike the cases considered

by Batchelor or Stewartson, the flow in Tesla turbine is not generated due to the rotation of the discs. The working fluid with both tangential and radial velocity enters through the small gap between the discs of finite size. This rotating flow generates torque on the discs' surfaces which leads to the rotation of the rotor. This study is also different from that of Bödewadt [38], because Bödewadt [38] had dealt with the case where there was a single static disc of infinite radius, the rotating fluid was of infinite expanse along the axis of rotation, and moreover there was no superposed inflow. The cases considered by some of the modern researchers like Poncet et al. [49] with superposed outflow is not applicable for Tesla turbine because they had considered a stator–rotor system but all discs in a Tesla turbine are rotors and the superposed flow is inward. None of the solutions given by Holodniok et al. [52,53], are applicable for a Tesla turbine because in all of their cases the discs are imparting rotation to the fluid. Another distinguishing feature of the Tesla turbine configuration is the small gap between two adjacent discs, which may be small enough in certain cases to be considered as a micro-channel. Usually the two boundary layers on the two discs would merge together, so that a core flow of the Batchelor-type does not occur. The boundary layers near the discs cannot also be described like the Ekman layer in which only Coriolis component of the inertial terms is retained.

Most of the previous researchers working in the field of the Tesla turbine have concentrated their attention on the engineering issues like control of operating parameters or design details; some of them have also given semi-empirical solutions. We have provided fundamental equations that govern the flow within the narrow gaps in a Tesla disc turbine and have explored the underlying science of various fluid dynamic behaviors. Thus the purpose of the present study is three-fold:

- (1) To provide a theoretical quantification of the three-dimensional fluid flow field that exists inside the small gap between two adjacent discs of the Tesla turbine. This is of scientific value since this new solution of rotating flow (with at least four distinguishing features, viz. that the fluid drives the solid surface, all solid surfaces rotate in the same direction, the inter-rotor gap is small and that there is a superposed inward flow) complements the previous scientific investigations on rotating flow discussed above.
- (2) Secondly, since this configuration of the rotating flow in a Tesla disc turbine has not been extensively studied previously, it is important to establish the scientific mechanisms and effects that each of the terms of the tangential and radial momentum equations gives rise to when they operate individually or together. The present study clarifies the role of inertial, centrifugal, Coriolis and viscous forces, identifying subtle mechanisms (e.g. the role of Coriolis force explained in Section 3.1 or the fact that the contribution of the r -component of viscous force to the overall radial pressure drop is extremely small (for air as working fluid) as explained in Section 3.4). To the best of our knowledge, such a complete assessment of the flow equations has not been previously performed in relation to the rotating flow within a Tesla disc turbine. This study has not only provided the relative importance of various terms under various operating conditions but also has elucidated the existence of subtle flow physics such as flow reversal (Section 3.2), the shape of the relative pathlines (Section 4) or the insensitivity of the quantity $\bar{V}_{\theta 1}$ at the flow outlet even when there is a large change in $\bar{V}_{\theta 2}$ varying from negative to positive values (Section 3.3). The detailed physical understanding is the scientific merit of the analysis and discussion given in Sections 3 and 4, which could not have been appreciated simply from a global, overall solution of all the equations in one go.

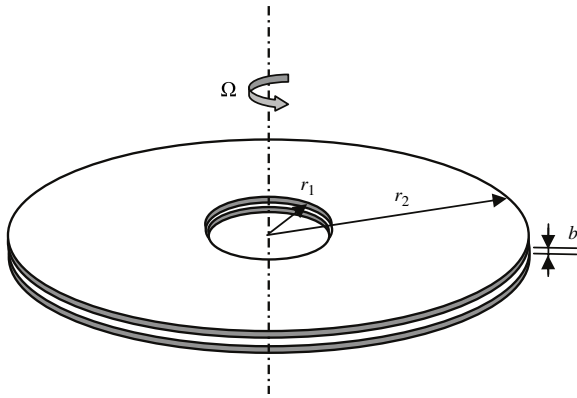


Fig. 1. Schematic diagram of the domain for the mathematical solution. (The gap within the two discs, in relation to the radius, is exaggerated in the sketch for clarity.)

(3) Thirdly, an analytical theory is presented for the calculation of the power output of the Tesla disc turbine, which has been validated against recent experimental measurements. From an engineering viewpoint, such a mathematical formulation gives one the rapid predictive power that a practicing engineer may need to design, optimize and analyze the machine. However, even if a Tesla turbine does not ultimately emerge as a valid engineering product, the mathematical solution has scientific value since it would characterize a type of turbomachinery, viz. the viscous flow turbine or Tesla disc turbine, for which an analogous theory did not exist before.

2. Outline of a theory for tesla disc turbines

The domain for the mathematical solution is the three-dimensional space (Fig. 1) between two circular rotor discs separated axially (i.e. in the z -direction) by a distance b . The rotor inlet is situated along the periphery of the discs (i.e. at radius r_2). The rotor outlet is at the center of the discs (at radius r_1).

The flow between the discs has been assumed to be steady, laminar and axisymmetric. In order to make the complex flow amenable to an analytical theory, a few more assumptions are made, which have been fully described by Sengupta and Guha [54]. The reference also includes a detailed order of magnitude analysis of the various terms of the three-dimensional conservation equations in the cylindrical coordinate system and based on these the appropriate important terms for the present problem are included in the governing equations given below.

Boyd and Rice [55] had shown that the ratio of axial component of velocity to the tangential or radial component of velocity is roughly of the order of b/r_2 . It is well-known that for a Tesla disc turbine the above ratio is very small. Therefore, the axial component is smaller than the other two components of velocities. Moreover, from the numerical solutions of Boyd and Rice [55] it can be found that above a certain value of the R (Radius ratio = r/r_2), that is $R > 0.5$, the axial component of velocity is almost zero. This estimate for the dimension of the inner radius (to avoid large outflow vortices [21]) is very often comparable to many of the practical design (for example in the configuration of Lemma et al. [13] $R_1 = 0.528$) of an efficient Tesla disc turbine. For this reason V_z has been neglected in the theory presented in the present article, this assumption makes the analysis simpler.

2.1. Governing differential equations and boundary conditions

The continuity equation, the momentum equations and boundary conditions are written in terms of relative velocities. For this

purpose the following relations between the absolute and relative velocities are used. $U_r = V_r$; $U_z = V_z$; $U_\theta = (V_\theta + \Omega * r)$. Depending on the assumptions mentioned above and an order of magnitude analysis, the simplified conservation equations take the following form.

Continuity equation

$$\frac{\partial V_r}{\partial r} + \frac{V_r}{r} = 0 \quad (1)$$

θ -Momentum equation

$$V_r \frac{\partial V_\theta}{\partial r} + \frac{V_r V_\theta}{r} + 2\Omega V_r = \nu \frac{\partial^2 V_\theta}{\partial z^2} \quad (2)$$

r -Momentum equation

$$V_r \frac{\partial V_r}{\partial r} - \Omega^2 r - 2\Omega V_\theta - \frac{V_\theta^2}{r} = -\frac{1}{\rho} \frac{dp}{dr} + \nu \frac{\partial^2 V_r}{\partial z^2} \quad (3)$$

z -Momentum equation

$$\frac{\partial P}{\partial z} = 0. \quad (4)$$

Boundary conditions

$$\text{at } r = r_2 \quad \bar{V}_r = \bar{V}_{r2} \quad \bar{V}_\theta = \bar{V}_{\theta2} \quad (5)$$

$$\text{at } z = 0, b \quad V_r = 0 \quad V_\theta = 0 \quad (6)$$

$$\text{at } z = b/2 \quad \frac{\partial V_r}{\partial z} = \frac{\partial V_\theta}{\partial z} = 0. \quad (7)$$

Within the boundary layer developed on the flat solid discs, the relative tangential and radial velocities at any radius between r_1 and r_2 can be modeled as

$$V_\theta(r, z) = \bar{V}_{\theta2} \zeta(R) G(z) \quad (8)$$

$$V_r(r, z) = \bar{V}_{r2} \xi(R) H(z). \quad (9)$$

Where, $R = \frac{r}{r_2}$, $\zeta(R) = \frac{\bar{V}_\theta(r)}{\bar{V}_{\theta2}}$, $\xi(R) = \frac{\bar{V}_r(r)}{\bar{V}_{r2}}$, $G(z) = \frac{V_\theta(r, z)}{\bar{V}_\theta(r)}$, $H(z) = \frac{V_r(r, z)}{\bar{V}_r(r)}$. G and H are respectively the z -variation of tangential and radial velocities within the boundary layers. Here we assume that the velocity profile of the fully developed flow is parabolic in nature. Accordingly, G and H are expressed as,

$$G = 6 \frac{z}{b} \left(1 - \frac{z}{b}\right) \quad (10)$$

$$H = 6 \frac{z}{b} \left(1 - \frac{z}{b}\right), \quad (11)$$

where b is the gap between the two discs. For a throughflow situation (i.e. when the inlet velocity is in the radial direction), Matveev and Pustovalov [56], Boyd and Rice [55], had assumed the same relation as Eq. (11) for the variation of the radial velocity. The results of a complete computational fluid dynamics (CFD) study [54] show that Eq. (10) adequately represents the velocity profile, particularly close to the disc wall (where the gradient of the velocity profile determines the wall shear stress).

2.2. Integration of the continuity equation

Eqs. (8) and (9) show that in order to determine V_r and V_θ completely, one needs to find out $\xi(R)$ and $\zeta(R)$. Integrating the differential form of the continuity Eq. (1), we can get $\xi(R)$.

$$\int_0^b \int_{r_2}^r \frac{\partial(rV_r)}{\partial r} \delta r \delta z = 0. \quad (12)$$

Eq. (12) leads to,

$$\xi(R) = \frac{\bar{V}_r(r)}{\bar{V}_{r2}} = \frac{r_2}{r}. \quad (13)$$

Lemma et al. [13] measured this variation in \bar{V}_{r2} and found that, for a particular pressure drop between the rotor inlet and the central exit, \bar{V}_{r2} is maximum when the rotor is stationary and its magnitude decreases linearly (up to 0.7 bar pressure drop) with Ω as given by:

$$-\bar{V}_{r2} = A - B\Omega. \quad (14)$$

In Eq. (14), A is the maximum inlet radial velocity for stationary rotor, and B is the slope to be determined by the ratio of the maximum inlet radial velocity for stationary rotor (A) to the rotational speed of rotor for which no flow condition is arrived at (Ω_0).

2.3. Integration of the r and θ momentum equations

We introduce the following three non-dimensional variables for further theoretical development:

$$p' = \frac{p - p_2}{\rho\Omega^2 r_2^2}, \quad \phi_2 = \frac{\bar{V}_{r2}}{\Omega r_2}, \quad \gamma = \frac{\bar{U}_{\theta 2}}{\Omega r_2}. \quad (15)$$

The θ -momentum Eq. (2) is integrated partially with respect to z over the domain $(0, b/2)$, giving:

$$\frac{d\zeta}{dR} = - \left\{ \frac{1}{R} + 10 \left(\frac{\nu}{\Omega b^2} \right) \frac{R}{\phi_2} \right\} \zeta - \frac{10}{6(\gamma - 1)}. \quad (16)$$

To avoid singularity of the solution of ζ at $\gamma = 1$ a new variable ζ_m is introduced, where $\zeta_m = \zeta(\gamma - 1)$

$$\frac{d\zeta_m}{dR} = - \left\{ \frac{1}{R} + 10 \left(\frac{\nu}{\Omega b^2} \right) \frac{R}{\phi_2} \right\} \zeta_m - \frac{10}{6}. \quad (17)$$

The r -momentum Eq. (3) is integrated partially with respect to z over the domain $(0, b/2)$, resulting in:

$$\frac{dp'}{dR} = R + 2\zeta_m + \frac{6}{5} \frac{\zeta_m^2}{R} + \frac{6}{5} \frac{\phi_2^2}{R^3} - 12 \left(\frac{\nu}{\Omega b^2} \right) \frac{\phi_2}{R}. \quad (18)$$

Eq. (14) is substituted in the Eqs. (17) and (18) and these two ODEs are solved for the initial conditions given below

$$\text{At } R = 1 : \zeta_m = \gamma - 1 \quad (19)$$

$$\text{At } R = 1 : p' = 0. \quad (20)$$

The solutions of the above two Eqs. (17) & (18) will give ζ_m and p' . Analytical solutions are possible and indeed have been derived. However, in this work, one objective is to find out the separate roles of various forces (Section 3.1), this is best done through numerical integration. Hence, the numerical integration procedure is elaborated in the next paragraph. The analytical solution of Eq. (17) gives the variation of V_θ :

$$\zeta = \frac{\frac{C_2}{C_1} + C_3 \exp \left[-\frac{C_1 R^2}{2} \right]}{R}, \quad (21)$$

where,

$$C_1 = \frac{10\nu}{\phi_2 \Omega b^2}, \quad C_2 = \frac{-10}{6(\gamma - 1)},$$

$$C_3 = \left(1 - \frac{C_2}{C_1} \right) \exp \left[\frac{C_1}{2} \right].$$

Analytical integration of Eq. (18), specifying p' , is found as a series solution and is lengthy. It is available in Ref. [54] and is not

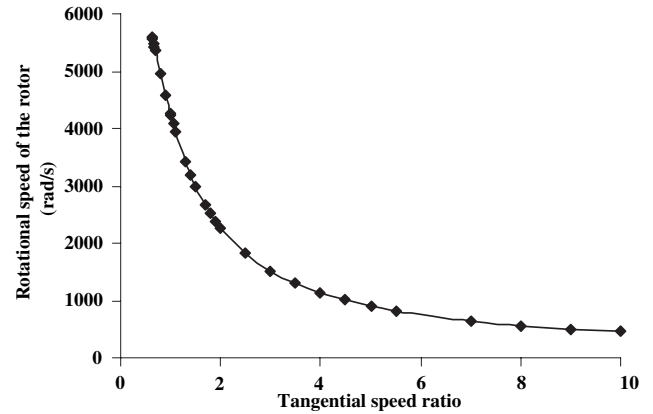


Fig. 2. Variation of steady rotational speed of the rotor (Ω_{steady}) versus tangential speed ratio γ : prediction of the presented theory. (For all calculations $\Delta p_{ic} = 0.113$ bar and air is used as the working fluid.)

reproduced here for the sake of brevity. It is instructive to note here that at the central exit, $p = p_2$, therefore $p' = 0$; at inlet, $p' = \Delta p_{ic}/(\rho\Omega^2 r_2^2)$. It is to be remembered that Lemma et al. [13] kept Δp_{ic} fixed for a given set of experiments; this is how the numerical predictions have been presented in various figures in order to be compatible with the experiments.

Eqs. (17) and (18) can also be integrated simultaneously by numerical means. A simple iterative scheme may be adopted as follows. Assume a value of γ for which the steady state solution is sought. Start with a trial value of Ω . Eqs. (17) and (18) are then numerically integrated from the rotor inlet to the central exit. The computed value of the pressure drop will not, in general, agree with the imposed value of Δp_{ic} . The value of Ω is then systematically varied until the iteration converges to the given value of Δp_{ic} . This converged value of Ω is the steady state value of the disc rotation for the given γ and Δp_{ic} : this value is denoted by Ω_{steady} . The same procedure is repeated for various values of γ . Fig. 2 gives the computed variation of Ω_{steady} with γ for a given Δp_{ic} ($\Delta p_{ic} = 0.113$ bar is chosen for the example calculation here because this value is used in the experiments of Lemma et al. [13]).

2.4. Calculation of torque and power output

From the known distribution in tangential velocity, the total torque and power output of the rotor can be calculated by the following steps.

Wall shear stress on one side of a single disc is given by,

$$\tau_w(r) = \left[\mu \frac{\partial V_\theta(r, z)}{\partial z} \right]_{at z=0} = \frac{6\mu\Omega r_2 \zeta_m}{b}. \quad (22)$$

Consider an elemental circular strip of thickness dr at a radius r . The torque about the rotor axis of the shear force acting on this elemental area is equal to $\tau_w(2\pi r dr)(r)$. The torque on one side of a single disc can be calculated by integrating the elemental torque, and is given by,

$$\begin{aligned} \mathfrak{S} &= \int_{r_1}^{r_2} \tau_w(2\pi r) r dr \\ &= \left(\frac{12\pi\mu\bar{V}_{\theta 2} r_2^3}{b} \right) \left[\frac{C_2}{C_1} (R_2^2 - R_1^2) \right. \\ &\quad \left. - \frac{C_3}{C_1} \left\{ \exp \left(-\frac{C_1 R_2^2}{2} \right) - \exp \left(-\frac{C_1 R_1^2}{2} \right) \right\} \right]. \quad (23) \end{aligned}$$

The net (integrated) effect of the jet on the disc becomes zero when $\int_{R_1}^{R_2} R^2 \zeta(R) dR = 0$; at this condition the jet produces no

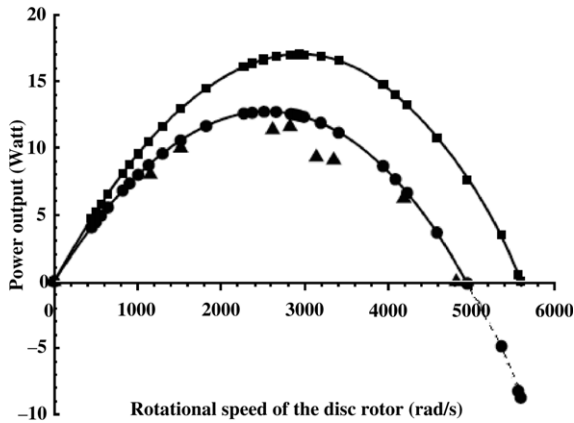


Fig. 3. Variation of the power output of Tesla turbine with rotational speed: comparison of the presented theory with experiment. (Keys: —■— Theoretical ideal power output, —●— Theoretical power output with loss, ▲ Experimental power output Lemma et al. [13]. Each bullet represents a steady state. For all calculations and experiments $\Delta p_{ic} = 0.113$ bar and air is used as the working fluid.)

torque, and hence no power. By substituting the expression for ζ given by Eq. (21) into this condition and performing the integration one can show that the no torque condition arises at a particular value of γ given by:

$$[\gamma]_{\text{no torque}} = 1 - \frac{10}{6} \left[\frac{C_1(R_2^2 - R_1^2) + \exp\left(\frac{C_1}{2}\right) \left\{ \exp\left(-\frac{C_1 R_2^2}{2}\right) - \exp\left(-\frac{C_1 R_1^2}{2}\right) \right\}}{C_1 \exp\left(\frac{C_1}{2}\right) \left\{ \exp\left(-\frac{C_1 R_2^2}{2}\right) - \exp\left(-\frac{C_1 R_1^2}{2}\right) \right\}} \right]. \quad (24)$$

The total torque produced by the complete rotor consisting of n_d discs is then calculated by,

$$\mathfrak{S}_{tot} = 2(n_d - 1)\mathfrak{S}. \quad (25)$$

The theoretical ideal power output is then given by,

$$\dot{W}_{th} = \mathfrak{S}_{tot} * \Omega. \quad (26)$$

Theoretical power output with loss can be calculated by subtracting the overall loss from \dot{W}_{th} given by Eq. (26):

$$\dot{W}_{act} = \dot{W}_{th} - \dot{W}_{loss}, \quad (27)$$

where, the loss is a function of Ω . An experimentally determined correlation for computing the overall loss is given [13]. A simple but very effective method for measuring the bearing and other losses, called the “angular acceleration method”, has been developed in [4].

The prediction of theoretical power output is shown in Fig. 3 for $\Delta p_{ic} = 0.113$ bar, where both the theoretical power outputs with and without loss are included. Each computed point in Fig. 3 represents a steady state solution. In the same figure the experimental results of Lemma et al. [13] are also shown so that a direct comparison is possible. An outer radius of 25 mm, an inner radius of 13.2 mm, and $n_d = 9$ were used in the experiments as well as in the calculations. Considering the facts that there is considerable experimental uncertainty and that the magnitude of the bearing and other losses is a very substantial fraction of the power output (see Fig. 3), it can be said that the simple theory developed here has worked well.

From simple theoretical considerations, Hoya and Guha [4] have shown that $\mathfrak{S} \approx \mathfrak{S}_0 - c\Omega$, where \mathfrak{S}_0 and c are constants, and

therefore the theoretical power output is $\dot{W}_{th} = \mathfrak{S}\Omega = \mathfrak{S}_0\Omega - c\Omega^2$. This explains why the power versus rotational speed curves in Fig. 3 show the general shape of inverted buckets and the power output produces a maxima. It can be seen that the rotational speed at which the maxima occurs is different for the two theoretical power output curves – the one which includes the loss and the other which does not. The experimental results of Lemma et al. [13] show that loss is proportional to the rotational speed. Eq. (27) therefore shows that $\dot{W}_{act} = \mathfrak{S}_0\Omega - c\Omega^2 - d\Omega$, where d is another constant. Hence the maxima for \dot{W}_{act} occurs at a lower rotational speed as compared to the maxima for \dot{W}_{th} . It is to be noted that measurements by “angular acceleration method” [4] showed that frictional torque, and hence the loss in power, can be a non-linear function of rotational speed; this aspect has been fully described in [54].

Fig. 3 shows that (for $\Delta p_{ic} = 0.113$ bar), the theoretical power output \dot{W}_{th} is zero at 5592 rad/s. This occurs when $\gamma = 0.631$, (this corresponds to the condition when there is no torque because of the action of the fluid jet on the disc). $\Omega_{\text{no torque}} = 5592$ rad/s thus corresponds to the steady state condition under no load. When the bearing and other parasitic losses are absent, the no torque condition, the no load condition and the no power condition all occur at the same steady rotational speed of the rotor. However, when bearing and other parasitic losses are present, an external agency will actually have to supply the power (that is equal to the losses) for the disc to rotate at the steady rotational speed of 5592 rad/s. This is shown as the negative power output in Fig. 3. The power output with losses becomes zero at 4950 rad/s, but at this point the torque produced by the jet is non-zero.

3. Role of various forces

3.1. The θ -momentum equation and the variation of V_θ

The θ -momentum Eq. (2) gives a balance of inertia force (L.H.S.) with friction force (R.H.S.) in the θ direction. In the inertial acceleration term $\left(V_r \frac{\partial V_\theta}{\partial r} + \frac{V_r V_\theta}{r} + 2\Omega V_r \right)$, $2\Omega V_r$ is the θ -component of Coriolis acceleration (henceforth denoted by $a_{c,\theta}$ for brevity). The term $\frac{V_r V_\theta}{r}$ takes an important part to conserve the angular momentum of the working fluid (henceforth denoted by a_H for brevity). The term $v \frac{\partial^2 V_\theta}{\partial z^2}$ represents the viscous (frictional) acceleration (henceforth denoted by $a_{f,\theta}$ for brevity), a negative value would show that it is in fact a deceleration. Eq. (2) may be interpreted as a relation that specifies the value of $\frac{\partial V_\theta}{\partial r}$, i.e. how V_θ changes with r . Depending on the relative magnitudes of $a_{c,\theta}$, a_H and $a_{f,\theta}$, $\frac{\partial V_\theta}{\partial r}$ may be positive, zero or negative. Thus, as one moves from the outer radius to the inner radius of a Tesla disc turbine, V_θ may show complex variation with the radius. We will attempt to analyze various scenarios in the following description.

It is easier to determine quantitatively the change in the value of V_θ with radius when the partial differential equation (2) is transformed into an ordinary differential equation (17). In Eq. (17), the four terms $\frac{d\zeta_m}{dR}$, $-\frac{\zeta_m}{R}$, $-\frac{10}{6}$ and $-10\zeta_m \left(\frac{v}{\Omega b^2} \right) \frac{R}{\phi_2}$ are derived respectively from $V_r \frac{\partial V_\theta}{\partial r}$, $\frac{V_r V_\theta}{r}$, $2\Omega V_r$ and $v \frac{\partial^2 V_\theta}{\partial z^2}$ of Eq. (2).

In Eq. (17), $\frac{d\zeta_m}{dR}$ gives the change in the value of ζ_m with non-dimensional radius R . Eq. (17) can be solved by a suitable numerical integration scheme (such as the finite difference method, FDM), if the value of ζ_m is known at a point. Eq. (19) shows that the initial value of ζ_m at rotor inlet (radius r_2) is $\gamma - 1$. It is recalled that the non-dimensional parameter γ , which is the ratio of the absolute tangential velocity of the fluid at rotor periphery and the peripheral speed of the rotor ($\gamma \equiv U_{\theta 2} / (\Omega r_2)$), has been introduced

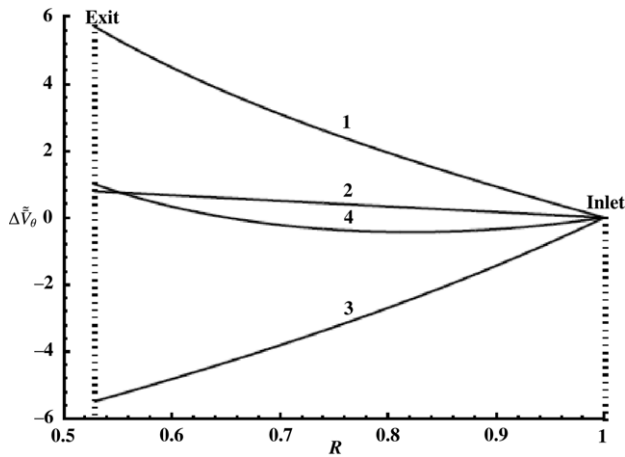


Fig. 4. Variation of $\Delta\tilde{V}_\theta$ from inlet ($R = 1$) to central exit ($R = 0.528$) for $\gamma = 10$: prediction of the presented theory. (Curve 1: Contribution of the term $V_r V_\theta / r$ in the variation of $\Delta\tilde{V}_\theta$, Curve 2: Contribution of the term $2\Omega V_r$ in the variation of $\Delta\tilde{V}_\theta$, Curve 3: Contribution of the term $v \frac{\partial^2 V_\theta}{\partial z^2}$ in the variation of $\Delta\tilde{V}_\theta$, Curve 4: Variation of $\Delta\tilde{V}_\theta$ considering all the forces. For all calculations $\Delta p_{ic} = 0.113$ bar and air is used as the working fluid.)

to incorporate different inlet flow conditions. The range from R_2 to R_1 is discretized into several grid points and ζ_m at each grid point can be calculated. The advantage of using FDM for solving Eq. (17) is that the contribution of each of the three terms in the RHS of Eq. (17) in determining the value of $\frac{d\zeta_m}{dR}$ at each grid point can be separately calculated.

There is a subtle point to be noted here. In the present FDM solution, the separate contributions of each of the three terms are calculated when all the three terms are present together, as in the actual case, in determining the variation of ζ_m from R_2 to R_1 . This is quite different from determining the effect of each term by first switching off the other two terms altogether in Eq. (17). A special example will clarify this subtlety. Suppose, the latter approach is taken and the value of γ is equal to 1. Therefore, $\bar{V}_{\theta 2} = 0$. Then, if one considered the effect of a_H alone, while neglecting the effects of $a_{C,\theta}$ and $a_{F,\theta}$, the value of \bar{V}_θ would remain zero at all radii (since $r_2 \bar{V}_{\theta 2} = r \bar{V}_\theta$ in this case). But in reality, due to the presence of a small radial velocity, a fluid particle moves towards the inner radius, \bar{V}_θ would change due to the Coriolis component $a_{C,\theta}$, and once the value of \bar{V}_θ becomes non-zero, it changes also due to the angular momentum conservation term a_H . The first calculation approach, the present finite difference method, would capture this subtle flow physics. Similarly, suppose $\bar{V}_{\theta 2} < 0$. Then, if one considered the effect of a_H alone, while neglecting the effects of $a_{C,\theta}$ and $a_{F,\theta}$, the value of \bar{V}_θ would remain negative at all radius (since $r_2 \bar{V}_{\theta 2} = r \bar{V}_\theta$ in this case). It is the effect of $a_{C,\theta}$ that makes the change over from negative to positive value of \bar{V}_θ possible (see ‘flow reversal’ discussed in Section 3.2). Fundamentally, the local value of overall \bar{V}_θ is important to find out the separate effects of each term because ζ_m also appears on the RHS of Eq. (17).

The value of \bar{V}_θ can be reconstructed from ζ_m by the transformation (using Eqs. (8) and (15)): $\bar{V}_\theta(r) = \Omega R \zeta_m(R)$. Figs. 4–6 show the contribution of each force in the non-dimensional variation of $\Delta\tilde{V}_\theta$ (or, the variation of $\Delta\tilde{V}_\theta$) with R for three different values of γ . The same figures also contain the net change of $\Delta\tilde{V}_\theta$ with R considering all forces acting along θ direction so that a comparative study can be performed.

At this point, a few general observations can be made regarding the influence of $a_{C,\theta}$, $a_{F,\theta}$ and a_H from Eq. (2). The rate of change of \bar{V}_θ with r due to the Coriolis component alone is -2Ω ; so $d\bar{V}_\theta/dr$ is

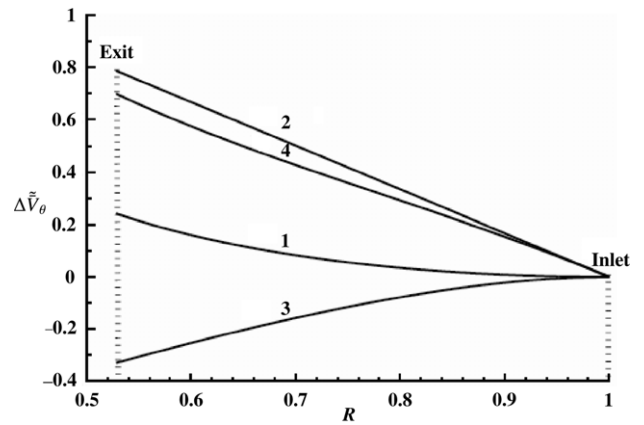


Fig. 5. Variation of $\Delta\tilde{V}_\theta$ from inlet ($R = 1$) to central exit ($R = 0.528$) for $\gamma = 1$: prediction of the presented theory. (Curve 1: Contribution of the term $V_r V_\theta / r$ in the variation of $\Delta\tilde{V}_\theta$, Curve 2: Contribution of the term $2\Omega V_r$ in the variation of $\Delta\tilde{V}_\theta$, Curve 3: Contribution of the term $v \frac{\partial^2 V_\theta}{\partial z^2}$ in the variation of $\Delta\tilde{V}_\theta$, Curve 4: Variation of $\Delta\tilde{V}_\theta$ considering all the forces. For all calculations $\Delta p_{ic} = 0.113$ bar and air is used as the working fluid.)

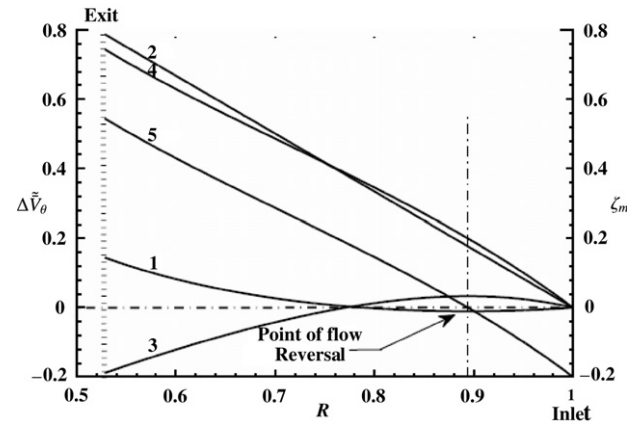


Fig. 6. Variation of $\Delta\tilde{V}_\theta$ from inlet ($R = 1$) to central exit ($R = 0.528$) for $\gamma = 0.8$: prediction of the presented theory. (Curve 1: Contribution of the term $V_r V_\theta / r$ in the variation of $\Delta\tilde{V}_\theta$, Curve 2: Contribution of the term $2\Omega V_r$ in the variation of $\Delta\tilde{V}_\theta$, Curve 3: Contribution of the term $v \frac{\partial^2 V_\theta}{\partial z^2}$ in the variation of $\Delta\tilde{V}_\theta$, Curve 4: Variation of $\Delta\tilde{V}_\theta$ considering all the forces. Curve 5: Variation of ζ_m ($\equiv \bar{V}_\theta / \Omega r_2$) considering all the forces. For all calculations $\Delta p_{ic} = 0.113$ bar and air is used as the working fluid.)

negative and constant at all radii. Therefore, as one moves from the rotor inlet to outlet (i.e. as r decreases), \bar{V}_θ increases along a straight line- this feature can be seen in each of the Figs. 4–6. The viscous force always acts against the relative speed \bar{V}_θ trying to diminish its magnitude – this feature can also be seen in each of the Figs. 4–6. When \bar{V}_θ is positive, the effect of the viscous force is simply to decrease the relative speed in the positive θ direction. Where \bar{V}_θ is negative (for example, in the region close to the rotor inlet when $\gamma < 1$), viscous force still tries to decrease the magnitude of \bar{V}_θ (in the negative θ direction) but this appears as an increase in \bar{V}_θ in the positive θ direction (see Fig. 6). The influence of a_H on $d\bar{V}_\theta/dr$ is complex and the nature of influence depends also on the value of γ . This has been explained below in the separate discussions on Figs. 4–6 (computed for $\gamma = 10, 1$ and 0.8 respectively).

Fig. 4 shows that while the θ -component of Coriolis acceleration ($a_{C,\theta}$) and $\frac{V_r V_\theta}{r}$ (i.e. a_H) tries to increase $\Delta\tilde{V}_\theta$, the viscous force tries to decrease $\Delta\tilde{V}_\theta$. As the value of \bar{V}_θ is high at $\gamma = 10$, the effect

of viscous force is also large. Fig. 2 shows that the steady value of the disc rotational speed Ω_{steady} is small at $\gamma = 10$; hence the magnitude of the Coriolis acceleration $a_{C,\theta}$ is small in comparison with the other two accelerations $a_{F,\theta}$ and a_H . For high values of γ , the present computations show that $a_{F,\theta}$ and a_H are comparable in magnitude but acts in opposite directions. Close to the rotor inlet, the effect of $a_{F,\theta}$ is greater, but as one moves to the rotor outlet (r_1) the combined effect of inertia terms ($a_H + a_{C,\theta}$) overtakes that of $a_{F,\theta}$. Hence, with decreasing r , $\Delta\tilde{V}_\theta$ initially decreases, then increases, as can be seen in Fig. 4.

Fig. 5 shows the effects of the three accelerations on the variation of $\Delta\tilde{V}_\theta$, when $\gamma = 1$. Like the case of $\gamma = 10$ shown in Fig. 4, Fig. 5 also shows that while the θ -component of Coriolis acceleration ($a_{C,\theta}$) and $\frac{V_r V_\theta}{r}$ (i.e. a_H) tries to increase $\Delta\tilde{V}_\theta$, the viscous force tries to decrease $\Delta\tilde{V}_\theta$, but there are very important differences. It is seen from Fig. 2 that at $\gamma = 1$, the value of Ω_{steady} is large, and hence the Coriolis acceleration, in this case (in contrast to the previously discussed case of $\gamma = 10$), becomes the dominant term. This dominance of the Coriolis term is evident in Fig. 5. There is also a difference in the nature of the curve 3 (i.e. the effect of the viscous acceleration $a_{F,\theta}$) between Figs. 4 and 5. It is observed that at $\gamma = 1$ the rate of decrease of \tilde{V}_θ with r (i.e. $d\tilde{V}_\theta/dr$) due to $a_{F,\theta}$ increases from R_2 to R_1 , whereas at $\gamma = 10$, the rate decreases from R_2 to R_1 . For $\gamma = 1$, the friction is zero at inlet (since the relative tangential velocity is zero at the rotor inlet), it increases rapidly from R_2 to R_1 . On the contrary, for a high value of γ , for example $\gamma = 10$, the friction at inlet is high and it changes slowly from R_2 to R_1 (the viscous force is proportional to the relative velocity of the fluid, and for $\gamma = 10$ the change of \tilde{V}_θ from R_2 to R_1 is small).

3.2. A novel case involving flow reversal

From a study of all previous references it would be a common expectation that, for the Tesla turbine to work, the absolute tangential speed of the fluid jet (situated at the rotor periphery) must be higher than the tangential speed of the rotor itself. This is synonymous to saying that the relative fluid tangential speed at rotor periphery $\tilde{V}_{\theta 2}$ must be positive, or equivalently $\gamma > 1$. During the present course of research it is discovered that, a Tesla turbine would also work even when γ is less than 1 (up to a point). It is found that the Coriolis acceleration is responsible for this subtle effect. It is recalled $a_{C,\theta}$ increases \tilde{V}_θ at a constant rate from R_2 to R_1 . Thus the action of the Coriolis acceleration has the capability to change \tilde{V}_θ from a negative value at R_2 to a positive value at R_1 , passing through the value of zero. This flow transition in the relative frame is possible only due to the effect of the Coriolis acceleration. (It can be shown that, starting from an initial negative value, \tilde{V}_θ would always remain negative due the individual effect of either a_H or $a_{F,\theta}$.) It was shown previously that, when the value of γ is near 1, the magnitude of $a_{C,\theta}$ dominates over the other two acceleration terms. Thus flow reversal in the relative frame becomes possible due to the Coriolis acceleration. In the region between the rotor inlet (R_2) and the point of flow reversal, the rotor disc would absorb power, instead of delivering. However, the disc would develop positive power in the region between the point of flow reversal and the rotor outlet (R_1). If the positive power is more than the negative power, then the rotor disc would produce a net power output and the Tesla turbine would remain functional. Obviously, from the present theory of produced net torque given in Section 2, one can determine the limiting value of γ (which is less than 1) for which the net torque of the Tesla turbine would just become zero. As per the knowledge of the present authors, this functionality of the Tesla turbine even when $\gamma < 1$ and the

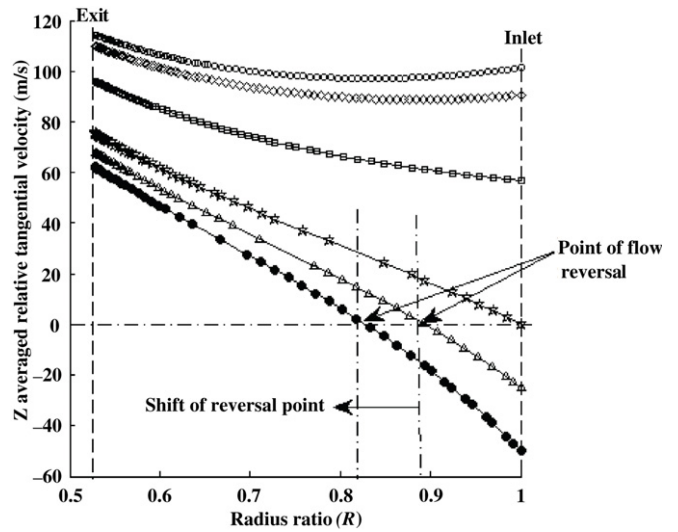


Fig. 7. Variation of z-averaged relative tangential velocity \tilde{V}_θ from inlet ($R = 1$) to central exit ($R = 0.528$): prediction of the presented theory. (Keys: $\gamma = 10$ ($\Omega_{steady} = 450$), $\gamma = 5$ ($\Omega_{steady} = 906$), $\gamma = 2$ ($\Omega_{steady} = 2273$), $\gamma = 1$ ($\Omega_{steady} = 4249$), $\gamma = 0.8$ ($\Omega_{steady} = 4950$), $\gamma = 0.64$ ($\Omega_{steady} = 5560$)). For all calculations and experiments $\Delta p_{ic} = 0.113$ bar and air is used as the working fluid.)

specific role of the Coriolis acceleration in achieving this have not been reported previously.

An example calculation for the functioning of a Tesla turbine with flow reversal is depicted in Fig. 6 for $\gamma = 0.8$. In this figure, an additional curve for the overall variation in non-dimensional \tilde{V}_θ (i.e. $\zeta_m \equiv \tilde{V}_\theta / \Omega r_2$) is also included so that the point of flow reversal can easily be identified.

It can be observed that the curve 1 (change in $\Delta\tilde{V}_\theta$ due to a_H) in Fig. 6 is completely different from the corresponding curves in Figs. 4 and 5. Moving from R_2 to R_1 , the curves 1 of Figs. 4 and 5 always move upward but the same curve in Fig. 6 goes downward from the rotor inlet to just before the point of flow reversal and it goes upward just after the point of flow reversal. This occurs because from the inlet to just before the point of flow reversal the value of ζ_m is negative and after that it becomes positive (angular momentum conservation tries to increase the modulus value of velocity).

Similarly, moving from R_2 to R_1 , the curves 3 (change in $\Delta\tilde{V}_\theta$ due to $a_{F,\theta}$) of Figs. 4 and 5 always move downward but the same curve of Fig. 6 first goes upward and then goes downward. This can also be explained by the flow reversal phenomenon. It is the nature of friction that it always acts against the direction of fluid flow; so from inlet to just before the point of flow reversal while \tilde{V}_θ is negative, friction tries to make \tilde{V}_θ positive and just after the point of flow reversal friction tries to make \tilde{V}_θ negative. At the point of flow reversal, the nature of curves 1 and 3 in Fig. 6 changes but the nature of curve 2 remains the same. It is so because the direction of the Coriolis acceleration remains unchanged. For the configuration of a Tesla turbine, V_r is always radially inward and the disc always rotates in the same direction (in the direction of the absolute velocity of the fluid jet). Hence, the vector generated from the cross product between Ω and V_r always acts in the same direction.

3.3. The net change in \tilde{V}_θ between the inlet and exit of the rotor

Fig. 7 shows the variation in \tilde{V}_θ with radius ratio, for various values of γ (10, 5, 2, 1.5, 1, 0.8, 0.64). $\gamma = 0.64$ corresponds to the near-no-torque condition. The complex features of the variation

in \bar{V}_θ and the reasons for such variations have been explained in Sections 3.1 and 3.2. It is found from Fig. 7 that the net change in \bar{V}_θ , i.e. $\Delta\bar{V}_\theta = \bar{V}_{\theta 1} - \bar{V}_{\theta 2}$, increases as the value of γ decreases. Thus, even when the value of \bar{V}_θ is quite small at rotor inlet (point 2), it increases to a large value at the rotor outlet (point 1). An example will clarify this important aspect. When $\gamma = 5$, $\bar{V}_{\theta 2} \approx 91$ m/s and $\bar{V}_{\theta 1} \approx 108$ m/s. When $\gamma = 1$, the relative tangential speed at rotor inlet is exactly zero, i.e. $\bar{V}_{\theta 2} = 0$. But the relative speed increases greatly within the rotor to assume a value of $\bar{V}_{\theta 1} \approx 75$ m/s at the rotor outlet. When $\gamma < 1$, $\bar{V}_{\theta 2}$ is negative, and yet $\bar{V}_{\theta 1}$ assumes a substantial positive value. This fluid dynamic behavior is interesting and important. (A comparison of the frictional curves in Figs. 4–6 shows that the magnitudes of the effect of friction at the rotor outlet are not very different from each other, considering that the value of γ has changed drastically from 10 to 0.8 among the three cases. The reason for this is the occurrence of high $\bar{V}_{\theta 1}$ in all cases.)

3.4. The r -momentum equation and the variation of pressure

Similar to the θ -momentum equation, the r -momentum equation (3) is also important in the fluid dynamics of a Tesla turbine. The role of various forces in the r -momentum equation is analyzed in this section. Some rearrangement of Eq. (3), using Eqs. (9) and (13), gives:

$$\frac{1}{\rho} \frac{dp}{dr} = \left(\frac{V_r^2}{r} + \frac{V_\theta^2}{r} \right) + \Omega^2 r + 2\Omega V_\theta + \nu \frac{\partial^2 V_r}{\partial z^2}. \quad (28)$$

In Eq. (28), $(V_r^2/r + V_\theta^2/r + 2\Omega V_\theta)$ is the inertial acceleration, $\Omega^2 r$ is the centrifugal acceleration, and $\nu \frac{\partial^2 V_r}{\partial z^2}$ is the viscous acceleration in the r -direction. In the following discussion, the term $2\Omega V_\theta$, which is the r -component of Coriolis acceleration, is separated from the total inertia term to judge its effect individually.

So, the present analysis is performed by considering the effects of the terms $(V_r^2 + V_\theta^2)/r$, $\Omega^2 r$, $2\Omega V_\theta$ and $\nu \frac{\partial^2 V_r}{\partial z^2}$ on the pressure drop. For the brevity of representation, the previous four acceleration terms are denoted respectively by the symbols $a_{I,r}$ (inertial), $a_{CF,r}$ (centrifugal), $a_{C,r}$ (Coriolis) and $a_{F,r}$ (viscous). The corresponding terms in the non-dimensional ODE (18), derived from the PDE (3), are respectively $(\frac{6}{5} \frac{\zeta_m^2}{R} + \frac{6}{5} \frac{\phi_2^2}{R^3})$, R , $2\zeta_m$, and $-12(\frac{\nu}{\Omega b^2}) \frac{\phi_2^2}{R}$. By multiplying the non-dimensional pressure drop with $\rho \Omega^2 r_2^2$ (from the definition of p' (15)) the dimensional pressure drop due to the effect of each force can be calculated.

It has been explained in Section 2.4 that, mimicking the experimental procedure of Lemma et al. [13], the pressure drop Δp_{ic} between the inlet and central exit of the rotor is kept fixed while obtaining various steady flow solutions and steady torque output conditions (see the computed combinations of γ and Ω_{steady} that give rise to the same pressure drop Δp_{ic} in Fig. 2). Fig. 8 shows an example calculation how the overall pressure occurs under the action of various forces over a wide range of Ω (for all the calculations the geometry of the turbine is taken to be the same as what is used in the numerical simulation of Section 2). Each point in Fig. 8 represents a steady state, hence although the symbol Ω is used in the following discussion on Fig. 8 to make it less cluttered, Ω actually refers to Ω_{steady} .

It can be seen from Fig. 8 that the pressure drop due to the inertia force $\rho a_{I,r}$ decreases with increasing disc rotational speed Ω . This is because \bar{V}_θ , at every value of the radius between the inlet and outlet, decreases as Ω increases, as shown in Fig. 7. Therefore $\rho V_\theta^2/r$ decreases with an increase of Ω . Though $|\bar{V}_r|$ decreases with Ω , the rate at which it decreases is very small because of the small value of B . (The values of A and B , corresponding to

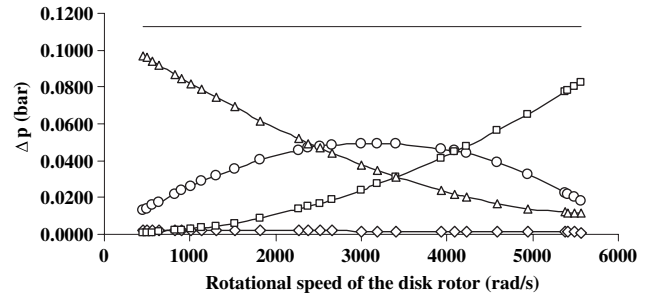


Fig. 8. Role of each force to produce a net pressure drop (Δp_{ic}) over a range of rotational speed of the rotor: prediction of the presented theory. (For all calculations $\Delta p_{ic} = 0.113$ bar and air is used as the working fluid. Keys: —○— Pressure drop due to Coriolis effect, —■— Pressure drop due to $\rho\Omega^2 r$, —◇— Pressure drop due to friction, —▲— Pressure drop due to $\rho(V_r^2 + V_\theta^2)/r$, — Total pressure drop.)

$\Delta p_{ic} = 0.113$ bar, are respectively 13.32 and 0.0014 according to Lemma et al. [13].)

The pressure drop due to the centrifugal force, $\rho a_{CF,r}$, increases with Ω . This is exactly opposite to the behavior due to the inertial force $\rho a_{I,r}$. Fig. 8 shows that, at high values of Ω the major portion of the pressure drop originates from the centrifugal force, and, at low values of Ω , the major portion of the pressure drop originates from the inertial force.

With increasing Ω , the pressure drop due to the r -component of Coriolis force, $\rho a_{C,r}$, first increases and then decreases. This is because $a_{C,r}$ is given by the product of Ω and V_θ . But it has been shown in the previous paragraph that \bar{V}_θ decreases when Ω increases. At first, the increase in Ω dominates the change in the value of the product, but eventually the decrease in \bar{V}_θ dominates. This is why, with an increase in Ω , the pressure drop due to $\rho a_{C,r}$ initially increases but then decreases after a certain value of Ω . It is interesting to note from Fig. 8 that the maximum value of pressure drop due to $\rho a_{C,r}$ occurs approximately around the value of Ω where the pressure drop curves due to $\rho a_{I,r}$ and $\rho a_{CF,r}$ intersect, indicating a change-over of relative importance of the latter two components.

Present computations show that the radial pressure drop due to viscous force $\rho a_{F,r}$ decreases continuously (nearly linearly) with increasing Ω . (This is due to the fact that $|\bar{V}_r|$ decreases with Ω .) A striking finding of the present study is that the contribution of the r -component of viscous force to the overall radial pressure drop is extremely small. This feature is evident from Fig. 8.

4. Computation of path line in the relative frame

The fluid has mainly tangential and a small radial component of velocities while it enters through the narrow gap between the discs. As a result, the fluid follows a spiral path from the inlet up to the central exit. If a computational fluid dynamics (CFD) software is used to simulate the flow-field in a Tesla disc turbine, pathlines can be obtained by Lagrangian tracking calculations. Pathlines can also be calculated from the presented analytical theory since it gives the three-dimensional variation of V_θ and V_r through the rotor passage. A code written by finite difference method is utilized to calculate a single path line from inlet to central exit for two different rotational speeds of the rotor. For computation of the pathline a plane is chosen where $V_\theta = \bar{V}_\theta$ and $V_r = \bar{V}_r$. The time taken by the working fluid to reach from inlet to central exit is divided into small steps. At each instant of time, \bar{V}_θ and \bar{V}_r can be calculated from the presented theory since the (r, θ) coordinate of the fluid particle is known from the numerical integration at the previous time step. As \bar{V}_r is known, the radial distance traveled by the fluid during a time step can be calculated and the change in the value of θ can be

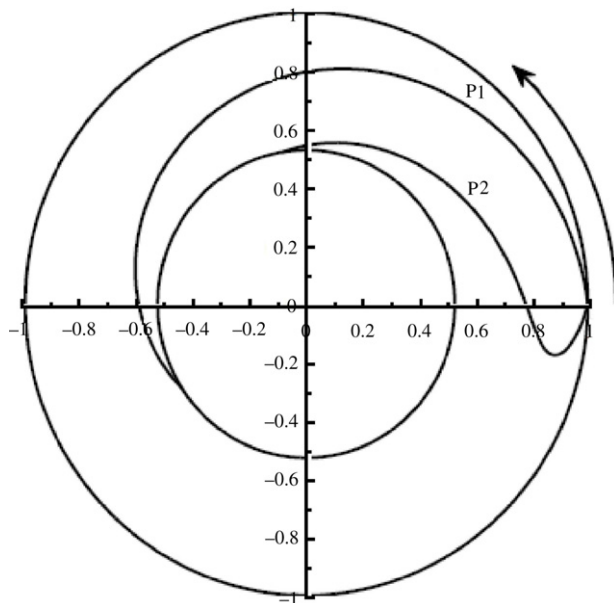


Fig. 9. Fluid path lines from inlet ($R = 1$) to central exit ($R = 0.528$) determined through numerical solutions of the presented theory for air as the working fluid and $\Delta p_{ic} = 0.113$ bar at two representative tangential speed ratios (γ). P1: Relative path line calculated at $\gamma = 10$, P2: Relative path line calculated at $\gamma = 0.8$ (arrow represents direction of rotation of the disc).

computed numerically from $\tan^{-1}(\bar{V}_r/\bar{V}_\theta)$. Successive application of this procedure enables one to trace the pathline (in the relative frame) completely from the inlet to the outlet.

The results are plotted in Fig. 9. The relative path line P1 of Fig. 9 shows that at $\gamma = 10$, the fluid moves spirally in the direction of the disc rotation (anticlockwise in the present example). The relative path line P2 of Fig. 9 shows that at $\gamma = 0.8$, a fluid particle first (i.e. in the inlet region) moves opposite to the disc rotation, then (near outlet region) it moves in the same sense as the disc rotation. This interesting shape of the pathline in the relative frame occurs due to the occurrence of flow reversal as detailed in Section 3. This fluid dynamic behavior is reported for the first time in this paper.

5. Conclusion

A theory for the rotating flow in the narrow gaps among closely-spaced co-axial multiple discs of a Tesla turbine is presented here. Both the θ -momentum and the r -momentum equations are considered. By a systematic order of magnitude analysis, the dominant terms have been retained in the governing conservation equations (1)–(3). This has made it possible to formulate analytical solutions and to develop a clear physical interpretation for each term in the equations. Thus the roles of each of the centrifugal, Coriolis, inertial and viscous forces in generating torque and power, and in establishing the pressure field have been comprehensively investigated and explained here. These physical roles of the individual forces have not been discussed previously in the literature.

The presented theory is simple but predicts three-dimensional fields of velocity and pressure. The torque and power output predicted by the theory compare well with recently published experimental results.

It is shown here that a Tesla disc turbine may generate net torque and power even when the tangential fluid speed at the disc periphery is less than the local tangential speed of the disc. The subtle role of the Coriolis acceleration in establishing such flow conditions, which involve flow reversal, has been explained.

Relative pathlines have been computed – it is shown that in addition to the usually reported spiral pathlines, new types of complex shaped path lines are formed when flow reversal occurs. The value of γ ($\equiv \bar{U}_{\theta 2}/\Omega r_2$) at which the theoretical torque becomes zero is given by an explicit relation – Eq. (24). The actual torque would become zero at a slightly higher value of γ than that given by Eq. (24) when the overall loss is taken into account.

Other than the existence of the phenomenon of flow reversal (Section 3.2), the subtle role of the Coriolis force in establishing flow reversal (Section 3.1) and the shape of complex relative pathlines (Section 4), the present study also reveals several other subtle flow physics. Some examples include the insensitivity of the quantity $\bar{V}_{\theta 1}$ at the flow outlet even when there is a large change in $\bar{V}_{\theta 2}$ varying from negative to positive values (Section 3.3) and the fact that the contribution of the r -component of viscous force to the overall radial pressure drop is extremely small (Section 3.4).

The net torque derived from the Tesla turbine is dependent on the viscous drag, which is a function of the axial (z -directional) gradient of relative tangential velocity. If one can favorably alter the shear stress (and hence power output) and control viscous and other losses, the Tesla turbine may emerge as a successful engineering device. This may be possible by using optimized values of overall dimensions and flow variables, and/or by intelligently manipulating local flow features. For example, it may be possible to exploit the effects of intelligently designed and manufactured surface roughness elements to enhance the performance of a Tesla disc turbine. We are not yet in a position to do so, but a thorough understanding of the fluid dynamics is a step in the right direction. The detailed physical understanding is the scientific merit of the analysis and discussion given in Sections 3 and 4, which could not have been appreciated simply from a global, overall solution of all the equations in one go.

References

- [1] N. Tesla, Turbine. US Pat. 1 061 206, 1913.
- [2] J.H. Armstrong, An Investigation of the Performance of a Modified Tesla Turbine, M.S. Thesis, Georgia Institute of Technology, 1952.
- [3] W. Rice, An analytical and experimental investigation of multiple-disk turbines, ASME Trans. J. Eng. Power 87 (1) (1965) 29–36.
- [4] G.P. Hoya, A. Guha, The design of a test rig and study of the performance and efficiency of a Tesla disc turbine, Proc. IMechE, Part A, J. Power and Energy 223 (A4) (2009) 451–465. DOI: <http://dx.doi.org/10.1243/09576509JPE664>.
- [5] A. Guha, B. Smiley, Experiment and analysis for an improved design of the inlet and nozzle in Tesla disc turbines, Proc. IMechE, Part A: J. Power and Energy 224 (2010) 261–277. DOI: <http://dx.doi.org/10.1243/09576509JPE818>.
- [6] W. Rice, Tesla turbomachinery, in: E. Logan (Ed.), Handbook of Turbomachinery, Marcel Dekker, New York, 2003, pp. 861–874.
- [7] A. Guha, Structure of partly dispersed normal shock waves in vapour-droplet flows, Phys. Fluids A 4 (7) (1992) 1566–1578.
- [8] A. Guha, Jump conditions across normal shock waves in pure vapour droplet flows, J. Fluid Mech. 241 (1992) 349–369.
- [9] A. Guha, A unified theory of aerodynamic and condensation shock waves in vapour-droplet flows with or without a carrier gas, Phys. Fluids A 6 (5) (1994) 1893–1913.
- [10] A. Guha, A unified theory for the interpretation of total pressure and temperature in two-phase flows at subsonic and supersonic speeds, Proc. R. Soc. Lond. Ser. A Math. Phys. Eng. Sci. 454 (1998) 671–695.
- [11] A. Guha, Computation, analysis and theory of two-phase flows, Aeronaut. J. 102 (1012) (1998) 71–82.
- [12] R. Steidel, H. Weiss, Performance test of a bladeless turbine for geothermal applications. Lawrence Livermore Laboratory, Report No. UCID-17068, 1974.
- [13] E. Lemma, R.T. Deam, D. Toncich, R. Collins, Characterisation of a small viscous flow turbine, J. Exp. Thermal and Fluid Sci. 33 (2008) 96–105.
- [14] L. Matsch, W. Rice, An asymptotic solution for laminar flow of an incompressible fluid between rotating disks, ASME Trans. J. Appl. Mechanics 35 (2) (1968) 155–159.
- [15] H.B. Schroeder, An investigation of viscosity force in air by means of a viscosity turbine. BAE Thesis, Rensselaer Polytechnic Institute, 1950.
- [16] W. Rice, An analytical and experimental investigation of multiple disk pumps and compressors, ASME Trans. J. Eng. Power 85 (1963) 191–198.

- [17] H.S. Couto, J.B.F. Duarte, D Bastos-Netto, The Tesla turbine revisited, in: 8th Asia-Pacific International Symposium on Combustion and Energy Utilization, October 10–12, Russian Federation, Sochi, 2006.
- [18] A. Valente, Installation for pressure reduction of hydrocarbon gases in a near isothermal manner. Abu Dhabi International Petroleum Exhibition and Conference, November 3–6; Abu Dhabi, UAE, 2008.
- [19] R.T. Deam, E. Lemma, B. Mace, R. Collins, On scaling down turbines to millimetre size, *ASME Trans. J. Engineering for Gas Turbines and Power* 130 (2008) 052301-1–052301-9.
- [20] V.P. Carey, Assessment of Tesla turbine performance for small scale solar Rankine combined heat and power systems, *Journal of Engineering for Gas Turbines and Power* 132 (12) (2010) art. no. 122301.
- [21] P. Lampart, K. Kosowski, M. Piwowarski, L. Jedrzejewski, Design analysis of Tesla micro-turbine operating on a low-boiling medium, *Polish Maritime Research* 1 (2009) 28–33 (special issue).
- [22] T.W. Choon, A.A. Rahman, F.S. Jer, L.E. Aik, Optimization of Tesla turbine using computational fluid dynamics approach, *Industrial Electronics and Applications (ISIEA), IEEE Symposium* (2011) 477–480. Langkawi.
- [23] N. Gregory, J.T. Stuart, W.S. Walker, On the stability of three dimensional boundary layers with application to the flow due to a rotating disk, *Philos. Trans. R Soc.* 248 (1955) 155–199.
- [24] A.J. Faller, R.E. Kaylor, Numerical study of the instability of the laminar Ekman boundary layer, *J. Atmos. Sci.* 23 (1966) 466–480.
- [25] Ö. Savas, On flow visualization using reflective flakes, *J. Fluid Mech.* 152 (1985) 235–248.
- [26] Ö. Savas, Stability of Bödewadt flow, *J. Fluid Mech.* 183 (1987) 77–94.
- [27] S.V. Pikhov, E.M. Smirnov, Boundary layer stability on a rotating disk with corotation of the surrounding fluid, *Fluid Dyn.* 27 (5) (1993) 657–663.
- [28] L. Schouveiler, P. Le Gal, M.P. Chauve, Stability of a traveling roll system in a rotating disk flow, *Phys. Fluids* 10 (1998) 2695–2697.
- [29] E. Serre, E. Crespo del Arco, P. Bontoux, Annular and spiral patterns in flows between rotating and stationary discs, *J. Fluid Mech.* 434 (2001) 65–100.
- [30] P.I. Sankov, E.M. Smirnov, Bifurcation and transition to turbulence in the gap between rotating and stationary parallel disks, *Fluid Dyn.* 19 (1985) 695–702.
- [31] G. Gauthier, P. Gondret, F. Moisy, M. Rabaud, Instabilities in the flow between co- and counter-rotating disks, *J. Fluid Mech.* 473 (2002) 1–21.
- [32] S. Murata, M. Yutaka, I. Yoshiyuki, A Study on a Disk friction pump, *Bull. Japan Soc. Mech. Eng.* 19 (136) (1976) 168–178.
- [33] P.S. Wu, Evaluation of Analytical Models for Multiple-Disk Pump Rotor Calculations. M.S. Thesis, Department of Mechanical and Aerospace Engineering, Arizona State University, 1986.
- [34] D. Nendl, Dreidimensionale laminare instabilitäten bei ebenen wänden, *Z. Angew. Math. Mech.* 56 (1973) T211–213.
- [35] D. Nendl, Reibungsturbine, *VDI-Ber. Nr.* 193 (1973) 287–293.
- [36] V.W. Ekman, On the influence of the earth's rotation on ocean currents, *Ark. Mat. Astron. Fys.* 2 (1905) 1–53.
- [37] T. von Kármán, Über laminare und turbulente Reibung, *Z. Angew. Math. Mech.* 1 (1921) 233–252.
- [38] U.T. Bödewadt, Die drehströmung über festem grunde, *Z. Angew. Math. Mech.* 20 (1940) 241–253.
- [39] G.K. Batchelor, Note on a class of solutions of the Navier–Stokes equations representing steady rotationally-symmetric flow, *Q. J. Mech. Appl. Math.* 4 (1951) 29–41.
- [40] K Stewartson, On the flow between two rotating coaxial disks, *Proc. Camb. Philos. Soc.* 49 (1953) 333–341.
- [41] K.G. Picha, E.R.G. Eckert, Study of the air flow between coaxial disks rotating with arbitrary velocities in an open or enclosed space, In *Proc. 3rd U.S. Natl Congr. of Appl. Mech.* 791–798, 1958.
- [42] G.N. Lance, M.H. Rogers, The axially symmetric flow of a viscous fluid between two infinite rotating disks, *Proc. R. Soc. A* 266 (1324) (1962) 109–121.
- [43] C.E. Pearson, Numerical solutions for the time-dependent viscous flow between two rotating coaxial disks, *J. Fluid Mech.* 21 (1965) 623–633.
- [44] A. Sirivat, Stability experiment of flow between a stationary and a rotating disk, *Phys. Fluids A* 3 (1991) 2664–2671.
- [45] G. Gauthier, P. Gondret, M. Rabaud, Axisymmetric propagating vortices in the flow between a stationary and a rotating disk enclosed by a cylinder, *J. Fluid Mech.* 386 (1999) 105–126.
- [46] D. Dijkstra, G.J.F. van Heijst, The flow between two finite rotating disks enclosed by a cylinder, *J. Fluid Mech.* 128 (1983) 123–154.
- [47] P.J. Zandbergen, D Dijkstra, Von Kármán swirling flows, *Annu. Rev. Fluid Mech.* 19 (1987) 465–491.
- [48] S. Poncet, M.P. Chauve, P Le Gal, Turbulent rotating disk flow with inward throughflow, *J. Fluid Mech.* 522 (2005) 253–262.
- [49] S Poncet, M.P. Chauve, R. Schiestel, Batchelor versus Stewartson flow structures in a rotor-stator cavity with throughflow, *Phys. Fluids* 17 (2005) 075110.
- [50] G.L. Mellor, P.J. Chapple, V.K. Stokes, On the flow between a rotating and a stationary disk, *J. Fluid Mech.* 31 (1968) 95–112.
- [51] M.H. Rogers, G.N. Lance, The rotationally symmetric flow of a viscous fluid in the presence of an infinite rotating disk, *J. Fluid Mech.* 7 (1960) 617–631.
- [52] M. Holodniok, M. Kubiček, V Hlaváček, Computation of the flow between two rotating coaxial disks, *J. Fluid Mech.* 81 (1977) 689–699.
- [53] M. Holodniok, M. Kubiček, V Hlaváček, Computation of the flow between two rotating coaxial disks: multiplicity of steady-state solutions, *J. Fluid Mech.* 108 (1981) 227–240.
- [54] S. Sengupta, A. Guha, A theory of Tesla disc turbines, *Proc. IMechE, Part A: J. Power and Energy* 226 (5) (2012) 650–663.
- [55] K.E. Boyd, W. Rice, Laminar inward flow of an incompressible fluid between rotating disks, with full peripheral admission, *ASME Trans. J. Appl. Mechanics* 35 (2) (1968) 229–237.
- [56] Y.Y. Matveev, V.N. Pustovalov, Calculation of laminar flow of a viscous fluid between rotating disks, *Izv. Akad. Nauk SSSR Mekh. Zhidk. Gaza* 1 (1982) 76–81. Translated from.